Catalysis Communications 181 (2023) 106728

Contents lists available at ScienceDirect

Catalysis Communications

journal homepage: www.elsevier.com/locate/catcom

Tuning the visible-light-driven photocatalytic properties of multi-decorated TiO_2 by noble metals towards both propionic acid and NOx degradation

Niloofar Haghshenas [a], Ermelinda Falletta [a,b,*], Giuseppina Cerrato [c], Alessia Giordana [c], Claudia L. Bianchi [a,c]

[a] Department of Chemistry, Università degli Studi di Milano, via C. Golgi 19, 20133 Milano, Italy
[b] Consorzio Interuniversitario Nazionale per la Scienza e Tecnologia dei Materiali (INSTM), via Giusti 9, 50121 Florence, Italy
[c] Department of Chemistry, University of Turin, Via Pietro Giuria 7, 10125 Turin, Italy

ARTICLE INFO

Keywords:
Photocatalysis
Noble metals decoration
Propionic acid
NOx
LED

ABSTRACT

Multiple noble metals-modified micrometric TiO_2-based photocatalysts were prepared by a cheap and sustainable approach based on the use of metal-enriched wastewaters (Ag, Au, Pt) and used for the photodegradation of propionic acid (PA) and NOx under LED. Properly tuning the metal decoration step, the material's photoactivity was optimized. 0.1%Pt @Ag/TiO_2 led to 60% PA removal, whereas the strong PA adsorption on the 0.1%Au @Ag/TiO2 surface caused a partial deactivation. In contrast, 0.1%Au @Ag/TiO_2 showed the highest photoactivity in the NOx decomposition (90%) due to the high tolerance of Au to HNO_3 produced on the catalyst surface.

1. Introduction

Unpleasant odors are the most disturbing pollutants and the main reason for air quality complaints in urban and industrial areas. Odor emissions consist of various chemical components, some of which can be perceived at very low threshold levels and significantly harm mental and physical health even at very low concentrations. [1] Volatile organic compounds (VOCs) have been designated the major odorant group. In particular, volatile fatty acids (VFAs) represent an important source of unpleasant odors that have been considered in many studies. [2] VFAs are mainly released from the anaerobic decomposition of organic waste in outdoor environments. However, there is a notable amount of these compounds in indoor areas as well, as a result of human activities. [3] Among VFAs, propionic acid (PA) has attracted much attention as one of the leading compounds responsible for odor-polluted areas. [4] Even if PA is generally considered a safe compound by the US Food and Drug Administration, it has shown specific toxicity in humans and other living organisms. [5]

On the other hand, nitrogen oxide (NOx) emissions represent one of the most hazardous air pollutants, causing various environmental and health problems. They contribute to ground-level ozone, global warming, acid rain, and urban smog. [6] Moreover, NOx exposure can lead to many respiratory and vision problems, lung dysfunction, and mental diseases.

Nowadays, many technologies are available for odors and NOx abatement and control. Among them, photocatalysis carried out under solar or artificial light has been widely applied to address many air pollution issues. [7]

Semiconductor-assisted photocatalysts permit to degrade of different types of pollutants without sludge formation and secondary pollutants production. It has been demonstrated that when a photocatalytic semiconductor is irradiated by light with an energy equal to or greater than the band gap energy of the material, electrons are promoted to the conduction band (CB) of the photocatalyst leaving holes in its valence band (VB). The so-produced photo-generated charges migrate onto the photocatalyst surface, reacting to adsorbed species and releasing reactive oxygen species (ROSs) responsible for the pollutants degradation. [8,9]

From the discovery of the water-splitting property of TiO_2 by Fujishima and Honda, [10] the applications of TiO_2 in water and air purification have multiplied due to its extraordinary properties, such as high stability, low cost, high availability, etc. In this regard, Betts et al. [11] investigated the photocatalytic activity of nano-sized TiO_2 (P25 Degussa) towards PA degradation under UV irradiation, demonstrating the high efficiency of the material. Similarly, many studies have been done to decompose NOx under UV light by pristine TiO_2. [7] To

* Corresponding author: Department of Chemistry, Università degli Studi di Milano, via C. Golgi 19, 20133 Milano, Italy.
E-mail address: ermelinda.falletta@unimi.it (E. Falletta).

https://doi.org/10.1016/j.catcom.2023.106728
Received 18 April 2023; Received in revised form 27 June 2023; Accepted 7 July 2023
Available online 12 July 2023
1566-7367/© 2023 The Author(s). Published by Elsevier B.V. This is an open access article under the CC BY-NC-ND license (http://creativecommons.org/licenses/by-nc-nd/4.0/).

overcome the limitation of TiO_2 and extend its photo-response to the visible region improving its photocatalytic performance, surface modification with noble metals nanoparticles (NPs) has been studied as an efficient approach. [12]

According to the literature, silver, platinum, and gold NPs are promising metals for this purpose. [13] These metal NPs exhibit localized surface plasmon resonances (LSPR), leading to a high Schottky barrier between metal and semiconductor that facilitates the electrons capture and, therefore, hinders the recombination rate between the electron and the holes. [14] Besides, some oxides, such as Ag_2O, formed during the synthesis can be coupled with TiO_2, enhancing the photoactivity and antimicrobial properties. [15]

Nevertheless, noble metals' high prices and resource shortage limit their applications. In fact, many studies aim to find alternatives based on cheaper and more abundant materials. [16] However, to date, noble metals recovery from wastewater from particular manufacturing processes has not been given much credit. However, this approach should be considered a valid progressive method to obtain the precursors of noble metal NPs at a low cost.

Many techniques have been proposed to produce noble metal nanoparticles, such as: biosynthesis, [17] chemical reductions of metal salts by traditional [18] and green approaches [19], and electrochemical methods. [20] Among all, electrochemical methods seem superior to obtain metal particles with higher purity and the possibility of particle size control.

Concerning the electrochemical approach, it has been demonstrated that the introduction of poly (N-vinylpyrrolidone) (PVP) as a protecting agent accelerates the metal particles formation on the cathode, making the electrochemical process more efficient (Chen et al. [21]). This technique was successfully applied by Stucchi et al. [22] to produce Ag NPs from a wastewater solution enriched in Ag^+ ions to decorate TiO_2 photocatalyst. However, it was recently demonstrated that a secondary decoration with other noble metals elevates the photoactivity of the catalyst [22], not only because it can overcome the possible restrictions related to the use of a non-pure precursor but also because the coupling of the two metals can lead to a positive synergistic effect. In this regard, some studies have reported Ag NPs stability enhancement when coupled with other noble metals, such as Au and Pt. [22] The synergistic effect between Au/Ag and Pt/Ag increases the localized surface plasmon resonance (LSPR) and, consequently, the electron trapping when compared to Ag/TiO_2 monometallic photocatalyst. [22]

In line with the global perspectives to enhance the efforts towards circular economy processes, the present research aims to synthesize multiple noble metals-modified micrometric TiO_2-based photocatalysts by a cheap and sustainable approach based on using metal-enriched wastewaters. The synthesized materials were applied in the photodegradation of PA and NOx, selected as model molecules for organic and inorganic air pollutants, respectively, under LED irradiation. The surface modification of TiO_2 was carried out by Ag as primary decoration, whereas Au, Pt, and bimetallic AuPt NPs were used as secondary decoration. In the present work, it is demonstrated that properly tuning the metal decoration step, the material's photoactivity can be optimized to enhance the activity towards propionic acid or NOx abatement.

2. Experimental

2.1. Materials

Micro-sized TiO_2 photocatalyst (1077, Kronos Worldwide, Inc.) is pure anatase, and its crystallographic structure was properly characterized in previous works of the research group. [23,24] Ag-enriched wastewater, as well as Au- and Pt-enriched wastewaters from Argor-Heraeus SA (Mendrisio, Switzerland), were used for primary and secondary decoration of TiO_2. The composition of the metal-enriched wastewaters is reported in Tables SI.1, SI.2, and SI.3. Other reagents, such as acetone (HPLC grade), sodium borohydride ((>98.0%), sulfuric acid (ACS reagent, 95.0–98.0%), propionic acid and D-(+) glucose (ACS reagent), were purchased from Sigma Aldrich, while 2-propanol (for analysis, ExpertQ, ACS reagent) was purchased from Scharlab and used without further purification.

2.2. Photocatalyst's preparation

2.2.1. Ag/TiO_2 synthesis (primary decoration)

Ag NPs were electrochemically synthesized in aqueous phase from the Ag-enriched wastewater by a method reported in the literature. [21]

More in detail, for the preparation of Ag/TiO_2, 1 g of TiO_2 was suspended in 2 mL of acetone. A proper amount of Ag NPs in the form of a colloidal solution was added to the previous suspension, and the mixture was stirred in a rotavapor (STEROGLASS, Strike 300) at 40 °C for 24 h. The temperature was increased to 80 °C for another hour until the complete solvent evaporation, obtaining a dried powder. The material was calcined in static air at 400 °C for 2 h. By this method $1\%Ag/TiO_2$, $4\%Ag/TiO_2$, and $8\%Ag/TiO_2$ photocatalysts were synthesized.

By the same procedure, an $8\%Ag/TiO_2$ photocatalyst ($8\%Ag/TiO_{2\text{-}pure}$)was prepared using an aqueous solution of Ag pure precursor ($AgNO_3$).

More details about the synthesis of the primarily decorated photocatalysts are reported in Table SI.4.

2.2.2. Metal @ag/TiO_2 synthesis (secondary decoration)

$8\%Ag/TiO_2$, which resulted in being the most efficient silver-decorated photocatalyst, was subjected to a secondary decoration by Au, Pt, and bimetallic AuPt NPs (with an Au/Pt ratio (wt./wt.) equal to 1). The synthesis was carried out through a wet impregnation method, as reported by Falletta et al. [25] A proper amount of Au- and Pt-enriched solution was added to ultrapure water. D- (+)-glucose (glucose/metal = 50:1 molar ratio) was added as a surfactant, followed by a few mL of 0.2 M $NaBH_4$ solution ($NaBH_4$/metal 1:1 (wt./wt.)) to obtain a colloidal dispersion. Eventually, the NPs were loaded on a proper amount of $8\%Ag/TiO_2$, quickly adjusting the pH to 3 by a 0.1 M H_2SO_4 solution. The mixture was maintained under stirring for 3 h. Finally, the acquired solid was recovered by filtration, dried at room temperature overnight, and calcined in air at 400 °C for 2 h. By this method, Au @Ag/TiO_2, Pt @Ag/TiO_2, and AuPt @Ag/TiO_2 were fabricated at different loading.

By the same procedure, a $0.1\%Au$ @Ag/TiO_2 and $0.1\%Pt$ @Ag/TiO_2 photocatalysts ($0.1\%Au$ @Ag/TiO_{2pure} and $0.1\%Pt$ @Ag/TiO_{2pure}) were prepared using aqueous solutions of Au and Pt pure precursors ($AuCl_4Na$ and Cl_4K_2Pt).

More details about the synthesis of the multi-decorated photocatalysts are reported in Table SI.5, SI.6, and SI.7.

The complete list of the synthesized materials is summarized in Table 1.

Table 1
List of the synthesized samples.

Material	Primary decoration	Secondary decoration	
	Ag%(wt.)	Pt%(wt.)	Au%(wt.)
$1\%Ag/TiO_2$	1	–	–
$4\%Ag/TiO_2$	4	–	–
$8\%Ag/TiO_2$	8	–	–
$8\%Ag/TiO_{2pure}$	8	–	–
$0.1\%Pt@Ag/TiO_2$	8	0.1	–
$0.5\%Pt@Ag/TiO_2$	8	0.5	–
$1\%Pt@Ag/TiO_2$	8	1	–
$0.1\%Au@Ag/TiO_2$	8	–	0.1
$0.1\%AuPt@Ag/TiO_2$	8	0.05	0.05
$0.1\%Pt@Ag/TiO_{2pure}$	8	0.1	–
$0.1\%Au@Ag/TiO_{2pure}$	8	–	0.1

2.3. Photocatalysts characterization

The specific surface area was determined by N_2 adsorption/desorption isotherms at 77 K (Tristar II 3020 (Micromeritics)) with Brunauer–Emmett–Teller (BET) and Barrett–Joyner–Halenda analyses. Before the analysis, the samples were pretreated ($T = 150$ °C, 4 h, N_2) to remove adsorbed foreign species. The synthesized sample's crystal structure and phase composition were recorded by X-ray powder diffraction (XRPD) on a Rigaku-Miniflex-600 diffractometer using monochromatic Cu- Kα radiation (λ = 1.541874 Å) at a scan rate of 0.02° min^{-1}.

UV–Vis diffuse reflectance (UV-DR) spectra were collected at room temperature (200–700 nm) by a double-beam UV–Vis–NIR scanning spectrophotometer (Perkin Elmer Lambda 750 s UV–Vis spectrophotometer, Perkin Elmer, Waltham, MA, USA), equipped with a diffuse reflectance accessory. The bandgap energy data were evaluated by performing the first derivative of the Kubelka-Munk transformation [26] according to Eq.1

$$F(R) = \frac{(1-R)^2}{2R} \quad (1)$$

where R is the reflectance. F(R) is proportional to the extinction coefficient (α). The modified Kubelka–Munk function can be obtained by multiplying the F(R) function by hν, using the corresponding coefficient (n) associated with an electronic transition as follows (Eq. 2):

$$(F(R) \times h\nu)^n \quad (2)$$

where h is the Planck's constant (J.s), ν is the photon frequency, n is the specific transition that can be experimentally determined from the best linear fit in the absorption spectra. [27]

The samples morphology and elemental analyses were evaluated using (i) a scanning electron microscope operating with a Field Emission source ((model TESCAN S9000G, (Overcoached, Germany); Source: Schottky type FEG; Resolution: 0.7 nm at 15 keV (in In-Beam SE mode) and equipped with EDS Oxford Ultim Max (operated with Aztec software 6.0). All samples have been coated with Cr by means of an ion sputtering technique to improve their conductivity; (ii) a transmission electron microscope operating in high-resolution mode (model JEOL 3010-UHR (Tokyo, Japan); acceleration potential: 300 kV; LaB6 filament) and equipped with an Oxford INCA X-ray energy dispersive spectrometer (X-EDS) with a Pentafet Si(Li) detector. Samples were dry dispersed before the investigation on Cu grids covered with Lacey carbon without any further treatment.

X-ray photoelectron spectroscopy (XPS) measurements were carried out on an M-probe apparatus equipped with an Al Kα source (hv = 1486.6 eV). Survey scans were measured between 0 and 1100 eV binding energy range with 5 eV energy resolution.

The photoluminescence at room temperature has been measured on solid samples using a Varian Cary Eclipse Fluorescence Spectrophotometer, exiting at 380 nm (slit ex = 5 nm, em = 5 nm).

2.4. Photocatalytic tests

2.4.1. Propionic acid photodegradation

Each sample was dispersed in 2-propanol and deposited onto glass support (10 × 10 cm) by drop-casting. The glass was placed inside a 5.5 L Pyrex reactor containing an initial 0.5 ppm concentration of PA in the vapor phase. The reactor was kept in the dark for 1 h to achieve the adsorption/desorption equilibrium, then irradiated by a LED lamp (350 mA, 9–48 V DC, 16.8 W) with an emission range of 400–700 nm, yielding 2800 LUX intensity on the catalyst surface for 180 min. The progress of the reaction was monitored by gas-chromatography (Shimazu GC-2025, FID detector, Column Teknokroma®, TRB-625, 30 m × 0.32 mm × 1.8 μm). Oven program: initial temperature 90 °C for 1 min, 70 °Cmin^{-1} up to 200 °C for 5 min. Flowrate: 3.00 mLmin^{-}1, SS inlet: Split mode (split ratio 5:0). Injector temperature: 200 °C; Detector temperature: 220 °C. Nitrogen was used as carrier gas.

To identify the PA transformation products (TPs), a gas-mass spectrometer (GC–MS, TRACE 1300 Thermo scientific, ISQ QD single quadrupole mass spectrometer Column VF-5 ms × 30 m) was used. Oven program: initial temperature 50 °C for 3 min, 10°Cmin^{-1} up to 100 °C for 2 min, 50 °Cmin^{-1} up to 200 °C. Flowrate: 3.00 mLmin^{-1}. Flowrate: 1.00 mLmin^{-1}; Purge flow: 5.0 mLmin^{-1}. Injector mode: splitless; Injector temperature: 200 °C. Helium was used as carrier gas. MS transfer line and ion source were both at 270 °C, Mass range: 45–500 amu.

2.4.2. NOx photodegradation

The photocatalysts that exhibited the most performing activity in the PA photodegradation (8%Ag/TiO_2, 0.1%Pt@Ag/TiO_2, 0.1%Au@Ag/TiO_2, and 0.1%AuPt@Ag/TiO_2) were selected for NOx degradation tests. Each material as solid powder dispersion in 2-propanol was deposited by drop-casting on glass support (20 cm × 2 cm) and placed in a 20 L Pyrex glass cylindrical reactor.

The reactor was filled in with NO_2 that partially decomposes into NO until the chemical equilibrium is obtained, with an initial concentration of 500 ± 50 ppb and maintained at 40–50% humidity.

The system was irradiated by a LED lamp (350 mA, 9–48 V DC, 16.8 W) with an emission range of 400–700 nm, yielding an intensity of 1000 lx on the catalyst surface. Both NO and NO_2 concentrations were instantaneously monitored during the reaction by an ENVEA AC32e chemiluminescence detector directly connected to the reactor.

3. Results and discussion

3.1. Materials characterization

The crystallographic phase composition of the synthesized samples has been characterized by X-Ray diffraction. The XRD patterns of all models (Fig. 1 A and B) show that both the primary and secondary decoration of TiO_2 does not affect the crystallographic phase of anatase, as expected according to the literature [24,28]. In contrast, the additional diffraction peaks at 38.1°, 44.3°, 64.4°, and 77.5 are associated with the 111, 200, 220, and 311 crystal planes due to Bragg's reflections for Ag NPs.

It is evident that in the XRD pattern of the 1%Ag/TiO_2 samples, the amount of metallic particles is too low to reveal, as well as for the metals used for the secondary decoration.

Moreover, the small peak at 32.5° observed in 0.1%Pt @Ag/TiO_2 sample can be associated with other metals present in the Pt-enriched solution used for the catalyst preparation, in particular two traces of Cr_3O_4, as Cr is the second metal more concentrated in the waste solution.

XPS survey analyses (Fig. SI.1) were carried out on the materials that showed the most promising photocatalytic properties (0.1%Pt @Ag/TiO_2, 0.1%Au @Ag/TiO_2), as well as on 0.1%AuPt @Ag/TiO_2 for comparison. The spectra exhibit the typical photopeaks associated with Ti2p, O1s, Ag3d, and C1s (284.6 eV), ascribed to adventitious carbon during XPS measurement.

The presence of Au and Pt, as well as other metallic impurities, were not detected because below the detection limit.

The high resolution (HR) C1s spectra (Fig. SI.2) show three components, C—C, C—O, and C═O, with a binding energy of 284.6, about 286.1, and 287.5, respectively.

The XPS HR spectra of Ti 2p, Ag 3d, and (d) O 1 s are displayed in Fig. 2.

Concerning Ti photopeaks, all samples show the presence of Ti(IV) (Fig. 2 A-C). In fact, the Ti 2p doublet can be seen, corresponding to 2p 1/2 and 2p 3/2 electrons, with doublet splitting of about 6 eV. Each signal can be deconvoluted into two peaks.

If compared to bare TiO_2 [29], the Ti 2p peaks of the synthesized materials are slightly shifted to higher binding energy values. In fact, the

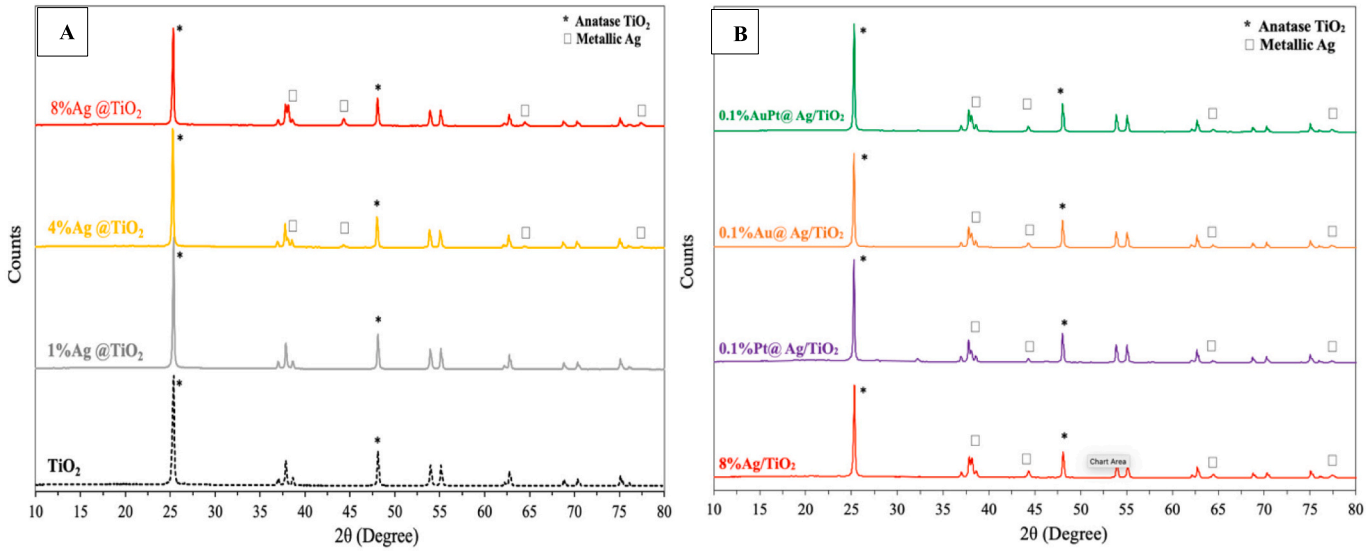

Fig. 1. XRPD patterns of both primary decorated (A) and secondary decoration (B) samples.

main peak of Ti 2p3/2 is centered at about 459 eV and is related to the Ti (IV) ions of bulk anatase, whereas the second peak at about 458 eV is associated to Ti(III) species, suggesting a strong interaction between Ag and Ti species. For all the samples, the HR XPS spectrum of O 1 s can be deconvoluted into three peaks (Fig. 2 G-I). The more intense photopeak, centered at about 529.3 eV, can be easily attributed to the crystal lattice oxygen (Ti-O-Ti), whereas that at ca. 531.2 eV is related to the presence of surface hydroxyl groups (Ti-OH) and finally the peak at about 533.5 eV is associated to adsorbed O_2. [29] The Ag 3d spectra of the materials consist of two individual peaks located at ca. 368 eV and ca. 374 eV, which should be assigned to Ag 3d5/2 and Ag 3d3/2 binding energies, respectively (Fig. 2 D—F). The peak at 368.0 eV is attributed to metallic silver (Ag^0). However, the Gaussian deconvolution of the Ag 3d5/2 signal of the 0.1%Au@Ag/TiO_2 leads to two peaks at 367.7 eV and 373.7 eV, assigned respectively to metallic silver and silver alloy, respectively. This second peak confirms the strong interaction between the two metals used for the TiO_2 decoration.

The optical properties of the prepared samples and their UV light absorption response were explored by diffuse reflectance spectroscopy (DRS) measurements. Fig. 3 (A and B) displays the Tauc plots and absorbance spectra of pristine TiO_2, 1%Ag@TiO_2, 4%Ag@TiO_2, and 8% Ag@TiO_2, respectively.

Although there is no significant shift in the bandgap energy of the decorated samples compared to the pristine TiO_2 (Table 2), they exhibited a notable absorption shift in the visible region (Fig. 3 B) that increases with the Ag NPs load. The UV–Vis absorption spectra of the Ag-decorated photocatalysts in the visible region are associated with the noble metal surface plasmon resonance (SPR) that increases the light absorption.

Concerning the doubly decorated samples, a further absorption shift in the visible region of the UV–Vis absorption spectra (Fig. 3 D) is observed, associated with the noble metals strong light absorption behavior due to the surface plasmon resonance (SPR).

However, although the bandgap energy values of the further Pt NPs-modified catalysts slightly decreased from 3.13 eV to 3.08 eV (Table 2), if compared to pristine TiO_2, this shift alone is not sufficient to justify the enhanced photoactivity of 0.1%Pt @Ag/TiO_2 towards PA degradation.

More in detail, comparing the UV–vis absorption spectra of 0.1%Pt @Ag/TiO_2, 0.5%Pt @Ag/TiO_2, and 1%Pt @Ag/TiO_2 (Fig. SI.3), it is evident that the maximum absorption values in the visible region are obtained for 0.1%Pt @Ag/TiO_2, according to the higher photoactivity of this sample towards the PA degradation reaction under LED.

This result could be associated with Pt NPs aggregation when the metal load exceeds a proper concentration.

Photoluminescence (PL) spectra of the most active samples (0.1%Pt @Ag/TiO_2, 0.1%Au @Ag/TiO_2), as well as on 0.1%AuPt @Ag/TiO_2 for comparison were performed, and the results are reported in Fig. 4.

The results are comparable to those reported in the literature for anatase titania. [30] The origin of PL spectra for the anatase phase is due to oxygen vacancies, self-trapped exciton, and surface states. The peaks, observed in the range 400–500 nm, are attributed to an indirect band gap, a surface recombination process, and self-trapped exciton (STE) localized on TiO_6 octahedra and oxygen vacancies on the surface area of TiO_2 nanoparticles. The visible emission (at 460, 485, and 520 nm) may be ascribed to the electron trapped in oxygen vacancies (the recombination of $e- / h+$ pair via oxygen vacancies). No extra PL component was shown by both primary or secondary decoration samples, suggesting that metal NPs may efficiently capture photoexcited electrons from TiO_2, providing a recombination route for the holes in TiO_2 particles that does not generate PL, in line with the results of Dozzi et al. [31]

The intensities of PL signals are indicative of the rate of $e-/h+$ recombination, so a lower intensity is related to a higher photocatalytic activity. [32] Comparing samples, the highest intensities are observed for 0.1%Au @Ag/TiO_2, which shows lower activity.

Neither the primary decoration nor the secondary one affects the values of the specific surface area (SSA) of the photocatalysts, as reported in Table 2.

The specific surface area of bare TiO_2 was measured 10 ± 2 m^2/g, and this value remained relatively unaffected for all the decorated samples.

For further morphological investigation, FESEM, HR-TEM, and EDS mapping were carried out for the doubly modified sample (0.1%Pt @Ag/TiO_2) that exhibited more promising photoactivity for both PA and NOx abatement and the corresponding one modified by single decoration (8%Ag/TiO_2).

Concerning primary decoration with 8%Ag NPs, the FESEM image (Fig. 5 A, secondary electrons (SE) signals) reports the typical characteristics of a micro-sized TiO_2 system, having a relatively inhomogeneous size distribution but always in the micro-dimension range (>100 nm). Fig. 8 B, referred to as the Back Scattered Electrons signals (BSE), evidences the presence of particles with different contrast that can be attributed to particles with different atomic numbers if compared to Ti and O species. Thus, being Ag the only other species, these might be attributed to Ag itself (average dimension range: above 200 nm).

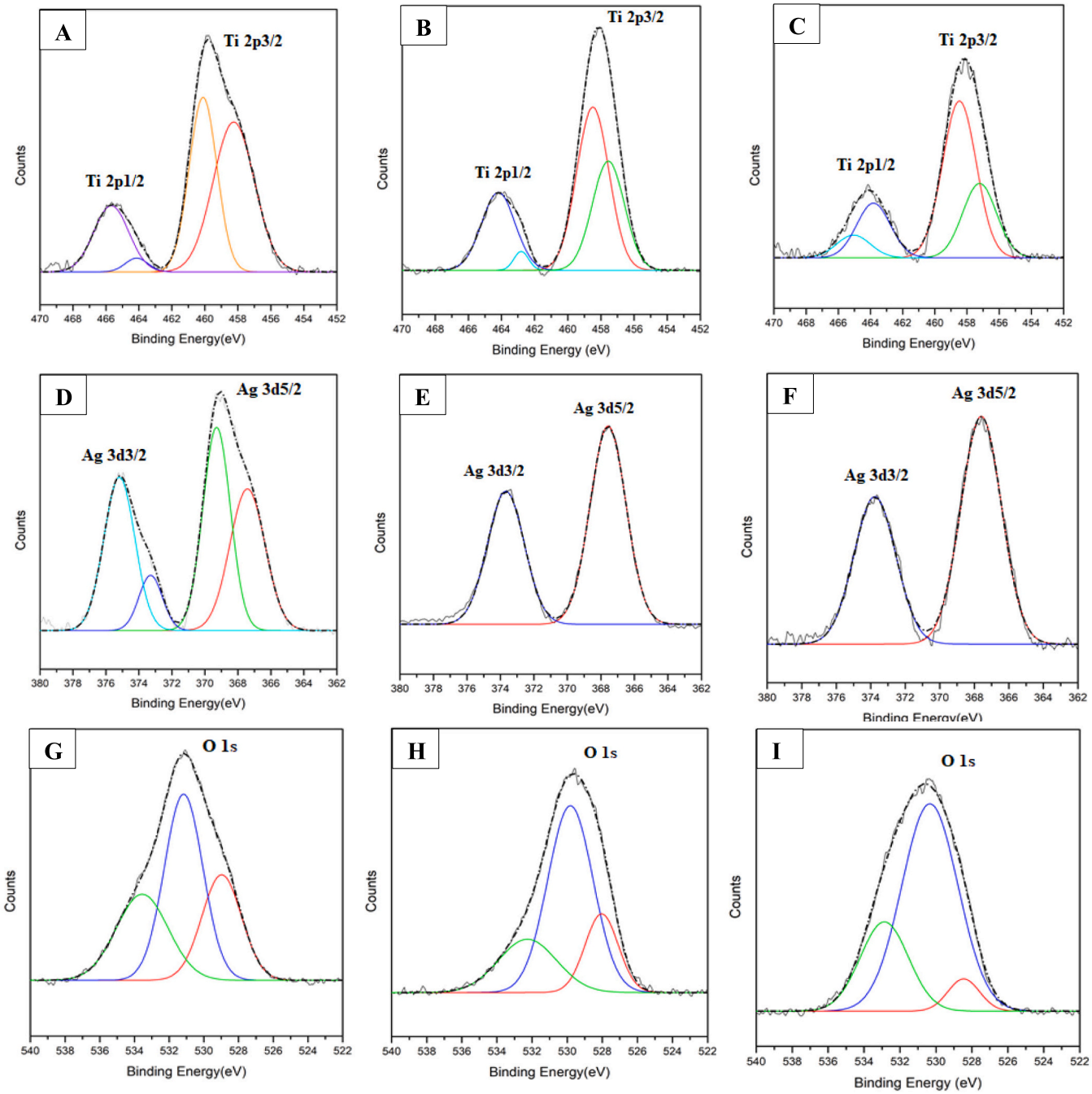

Fig. 2. XPS HR spectra of Ti 2p (A, B, and C), Ag 3d (D, E, and F), and O 1 s (G, H, and I) of samples: 0.1%Au @Ag/TiO_2, 0.1%Pt @Ag/TiO_2, and 0.1%AuPt @Ag/TiO_2 respectively.

The EDS analysis (Fig. 5 C) and the elemental mapping (Fig. 5 D) confirm this qualitative assumption and give both the quantitative indication, being Ag percentage very close to the theoretical one (~8% wt), and the arrangement relative to the Ag species. If the 8%Ag/TiO_2 sample is inspected in deeper detail (i.e., at higher magnification; see, for instance, Fig. 5 E and F), it is evident that there are also individual Ag particles of relatively limited size (from 20 to 80 nm, with shapes that are not always spherical): also, in this case, the mapping (Fig. 5 G) confirms this feature.

Fig. 6 reports the results obtained for the 0.1%Pt @Ag/TiO_2 material. Although the system is basically very similar to the 8%Ag/TiO_2 sample previously described, the presence of particles characterized by higher contrast is evident: these particles are rather heterogeneously dispersed on the top of the TiO_2 matrix and might be attributed to both metals added in the preparatory phase (i.e., Ag and Pt species). FESEM (Fig. 6 A) and HR-TEM (Fig. 6 C and D) images indicate that there are two-dimensional regimes in which the metallic particles were observed: one is significantly larger (> 15 nm), whereas the other exhibits smaller dimensions in the order of a few nm (2–4). The bimodal size distribution of the NPs is particularly evident in the BSE signal image (Fig. 6 B).

As reported in the literature, [33] particle accumulation, non-homogeneous size, and low dispersion can be associated with long-term materials exposure at high temperatures during the calcination step. In fact, the samples synthesized with a multi-decoration approach were distressed by multi-step calcination, applied after each metal decoration.

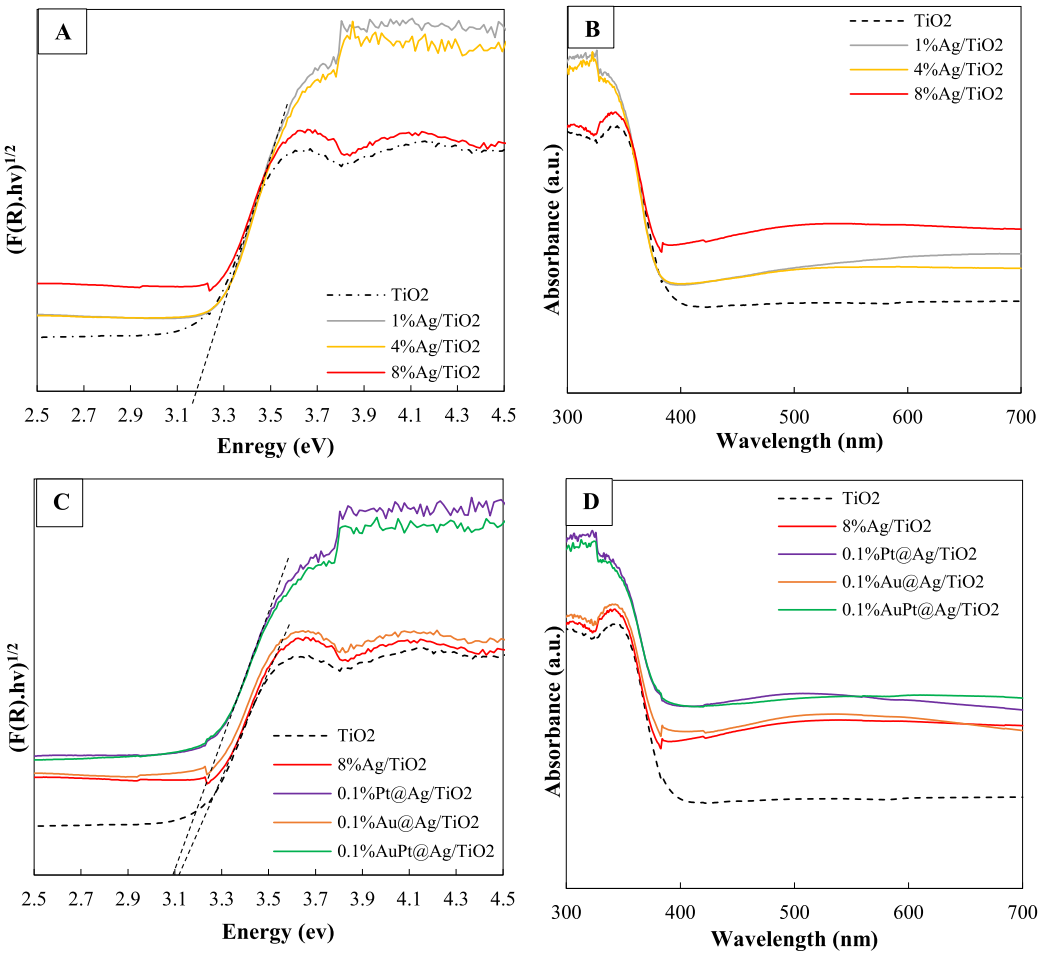

Fig. 3. Tauc plots (A and C) and the UV–Vis absorption spectra (B and D) of all synthesized samples.

Table 2
SSA and band gap energy values of pristine TiO_2, Ag/TiO_2, 0.1%Pt $@Ag/TiO_2$, 0.1%Au $@Ag/TiO_2$ and 0.1%AuPt $@Ag/TiO_2$.

Sample	SSA(m^2/g)	Bandgap (eV)
TiO_2	11	3.13
1%Ag/TiO_2	11	3.15
4%Ag/TiO_2	9	3.15
8%Ag/TiO_2	9	3.12
0.1%Pt$@Ag/TiO_2$	10	3.08
0.1%Au$@Ag/TiO_2$	12	3.10
0.1%AuPt$@Ag/TiO_2$	10	3.08

Although the EDS investigation confirms that the percentage of Pt was close to the theoretical one (~0.1%wt), the estimated amount of Ag particles in the investigated zone was much lower than the theoretical one, which can be the result of the non-homogeneous distribution of Ag metal NPs on the surface of TiO_2, as explained above.

The co-presence of these two metal NPs can form a heterojunction between them and increase the possibility of synergistic effects.

3.2. Photocatalytic results

The photocatalytic properties of the synthesized materials were evaluated by the decomposition of PA and NOx, selected as model molecules for organic and inorganic air pollutants, respectively, under LED irradiation.

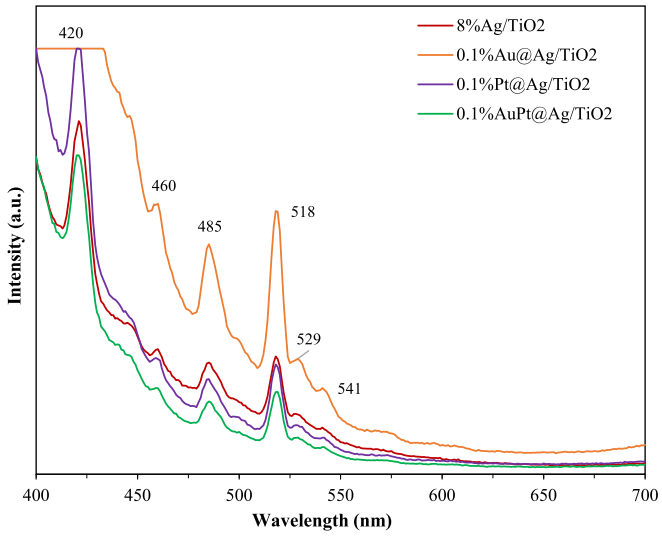

Fig. 4. PL spectra of 8%Ag/TiO_2, 0.1%Au $@Ag/TiO_2$, 0.1%Pt $@Ag/TiO_2$, 0.1% AuPt $@Ag/TiO_2$ (λ_{exc} = 380 nm).

3.2.1. Propionic acid photodegradation

Fig. 7 reports the results of the PA photodegradation by all the synthesized catalysts.

As can be seen in Fig. 7 A, the photolysis test led to a 20% PA decomposition in 3 h. Monitoring the reaction by GC/MS technique,

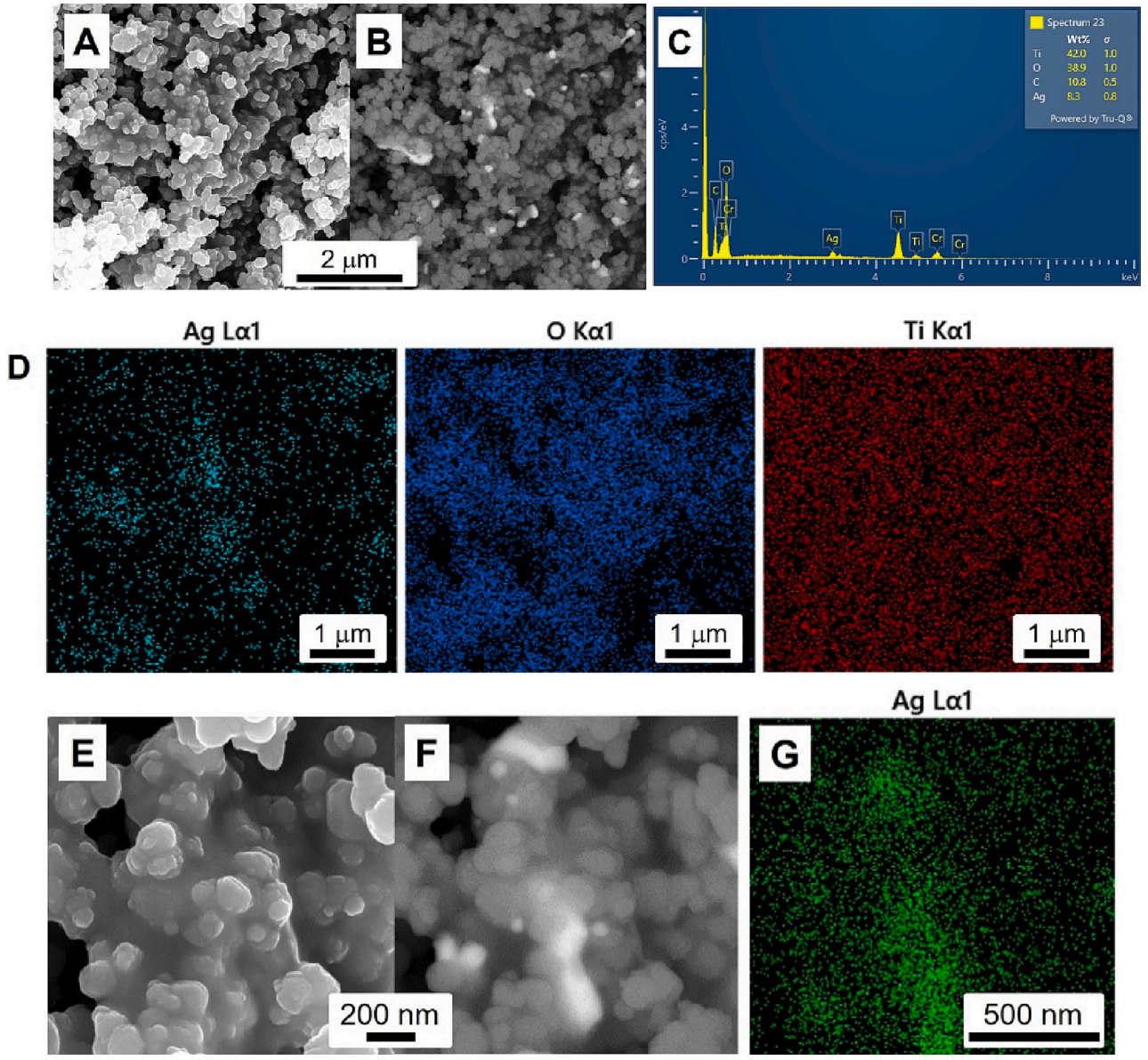

Fig. 5. FESEM SE (A and E) and BSE (B and F) images, EDS spectrum (C), and elemental mapping (D and G) of 8%Ag/TiO_2 photocatalyst.

glycolic acid and glyoxylic acid were identified as primary degradation products, as already observed in previous studies. [11]

Concerning the photodegradation tests, if, on the one hand, the bare TiO_2 shows a very poor photoactivity, starting after 90 min of irradiation, on the other hand, as expected, [24,28] Ag/TiO_2 leads to a pronounced increase in photoactivity (Fig. 7 A).

The photoactivity of the Ag-decorated photocatalysts is associated with the strong light absorption behavior of noble metal due to its localized surface plasmon resonance (LSPR), derived from the collective oscillation of surface electrons. Besides, the metal/semiconductor Schottky junction can facilitate the e^-/h^+ separation for charge transfer. [34]

Moreover, the increase of Ag NPs load on the surface of TiO_2 up to 8% led to a beneficial effect on photoactivity, especially in the first 90 min of irradiation. In fact, after about 1 h, the 8%Ag/TiO_2 photocatalyst is able to decompose more than 30% of PA. In addition to the best photocatalytic performance, such a high quantity of Ag should guarantee useful antibacterial properties of the material surface. A further increase in the metal load would, on the one hand, would lead to surface aggregation of the NPs with negative effects on the photocatalytic properties and higher process costs for the synthesis. For this reason, this material was selected for further decoration (secondary decoration), as described above.

Fig. 7 B shows that, if compared to 8%Ag/TiO_2, the second decoration with Pt NPs (0.1%Pt@Ag/TiO_2) causes a strong enhancement in the PA degradation, leading up to 60% of its removal in 180 min. In contrast, by using Au NPs (0.1%Au@Ag/TiO2) for the secondary decoration, the photoactivity of the material was worsened (40%) even compared to 8%Ag/TiO_2.

Finally, as for the bimetallic secondary decoration, 0.1%AuPt @Ag/TiO_2 photocatalyst caused no photocatalytic activity improvement if compared to 8%Ag/TiO_2. In fact, the promoting effect due to the presence of Pt NPs is balanced by the deactivation phenomena related to the presence of Au NPs.

The photoactivity enhancement of 0.1%Pt @Ag/TiO_2 can be attributed to the synergistic effect between Ag/Pt that promotes the separation of photogenerated e^-/h^+ through trapping electrons and improving the quantum efficiency. [35] The localized surface plasmon resonance (LSPR) effect from Ag NPs and the “electron sink” effect from Pt NPs makes 0.1%Pt@Ag/TiO_2 an efficient photocatalyst. [36]

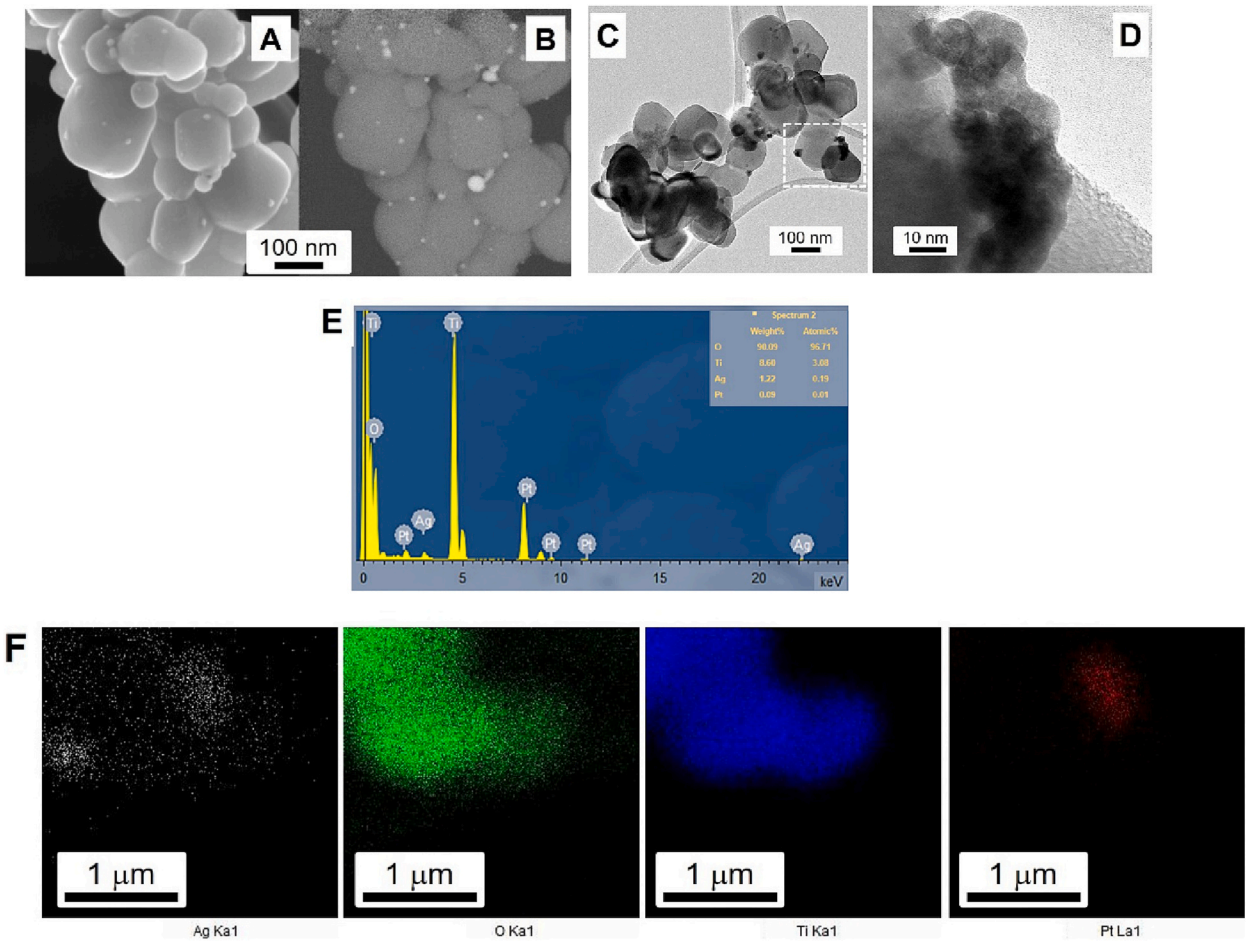

Fig. 6. FESEM SE (A), BSE (B), HR-TEM (C and D) images, EDS spectrum (E)and elemental mapping (F)of 0.1%Pt@AgTiO$_2$ photocatalyst.

On the contrary, if compared to the other materials 0.1%Au @Ag/TiO$_2$ shows a strong initial deactivation. This result is related to the strong surface adsorption of propionic acid molecules that blocks the active sites reducing their photoactivity. In fact, to prove this hypothesis, the catalyst was exposed to propionic acid vapor for 2 h in the dark and then exposed to LED irradiation for the photodegradation tests. The results confirmed that, after such a prolonged exposure time to PA vapors, the catalyst undergoes an important deactivation (Fig. SI.5).

In order to investigate the effect of the metal impurities on the photocatalysts prepared by the metal-enriched wastewater, similar materials were fabricated by the use of Ag, Pt, and Au pure precursors, and the photocatalytic results are reported in Fig. SI.6.

Surprisingly, if compared to the results reported in Fig. 5A, the data obtained by the photocatalysts synthesized using pure precursors are poor, although a similar trend can be observed (0.1%Pt@Ag/TiO$_2$ > 8% Ag/TiO$_2$ > 0.1%Au@Ag/TiO$_2$). 8%Ag/TiO$_2$ prepared by a pure precursor (8%Ag/TiO$_{2pure}$) degrades less than 30% of PA after light irradiation (3 h). A comparison of the XRD patterns of the 8%Ag-modified photocatalysts (8%Ag/TiO$_{2pure}$ and 8%Ag/TiO$_2$, 4%Ag/TiO$_2$ and 1% Ag/TiO$_2$) is shown in Fig. SI.7. First of all it is possible to observe that the peaks related to Ag NPs are less intense in the XRD pattern of 8%Ag/TiO$_{2pure}$, demonstrating that this material contains a smaller amount of Ag. Moreover, in the XRD pattern of 8%Ag/TiO$_2$ other peaks appear that can be attributed to the impurities of the waste solution.

It is evident from these results that the impurities present in the Ag-enriched waste (mainly Cu) have positive effects on the photocatalytic properties of the materials, very probably reducing the holes-electrons recombination and, consequently, enhancing the lifetime of the photogenerated charges.

In this regards, the higher activity of Cu-co-doped Ag/TiO$_2$ photocatalysts compared to Ag/TiO$_2$ have demonstrated in the literature. [32]

Fig. SI.8 shows the time-resolved profiles of the transformation products (TPs) obtained during the PA photodegradation carried out in the presence of both 0.1%Pt @Ag/TiO$_2$ and 0.1%Au @Ag/TiO$_2$ and monitored by GC. It can be noticed that the common TPs when each 0.1%Au @Ag/TiO$_2$ or 0.1%Pt @Ag/TiO$_2$ is used follow a different time-resolved profile.

In order to identify the TPs produced during the PA photodegradation process, the reaction carried out by both 0.1%Pt @Ag/TiO$_2$ and 0.1%Au @Ag/TiO$_2$ was monitored by GC/MS. Only some of the TPs observed by GC analysis were identified, and based on this result, a hypothesis of the PA photodegradation pathway was proposed (Scheme 1).

The PA photodegradation pathway by nanometric TiO$_2$ (P25 Degussa) under UVA irradiation was already described by Lynn M. et al. [11] According to this study, the PA photodecomposition proceeds through competitive and consecutive reactions that form acetic acid, ethanol, and acetaldehyde.

If compared to the literature, a new TP is here identified corresponding to ethyl propionate, most likely arising from not degraded propionic acid and ethanol (Scheme 1).

Considering the beneficial effect of the Pt NPs as the secondary decoration on 8%Ag/TiO$_2$, two further photocatalysts were synthesized, for which the percentage of Pt NPs was increased from 0.1% to 0.5% and 1% wt. and tested for the PA photodegradation (Fig. 7 C).

As shown in Fig. 7 C, the increase in Pt NPs load negatively affects the activity of the photocatalysts. This result was expected according to the UV–Vis absorption spectroscopy of these samples (Fig. SI.3) and could

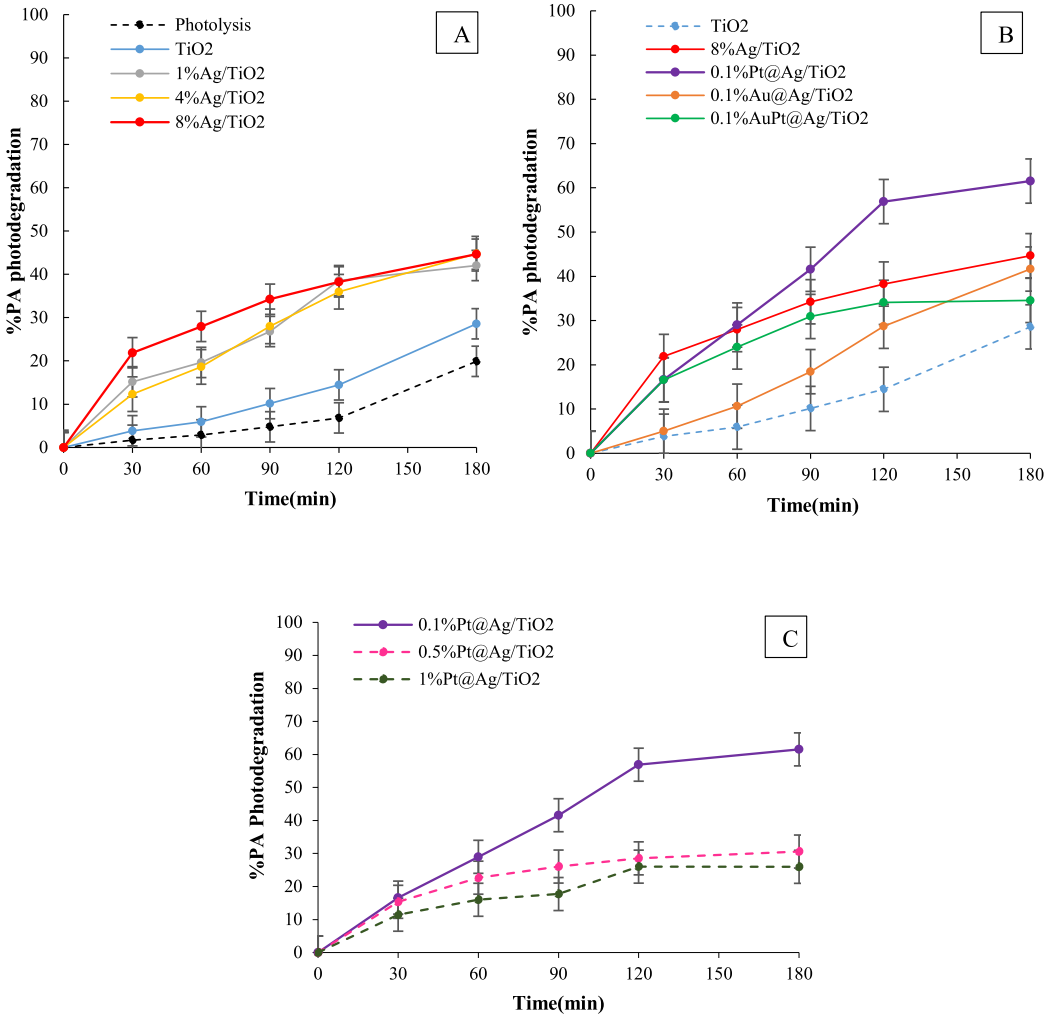

Fig. 7. Percentage of PA photodegradation using TiO_2, 1%Ag/TiO_2, 4%Ag/TiO_2 8%Ag/TiO_2 (A), TiO_2, 8%Ag/TiO_2, 0.1%Pt @Ag/TiO_2, 0.1%Au @Ag/TiO_2 and 0.1% AuPt @Ag/TiO_2 (B), And 0.1%Pt @ Ag/TiO_2, 0.5%Pt @ Ag/TiO_2 and 1%Pt @ Ag/TiO_2 (C).

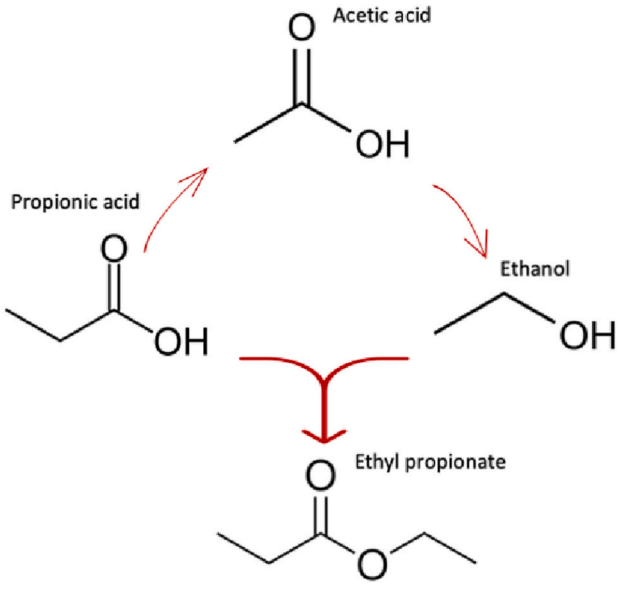

Scheme 1. Proposed photodegradation pathway for propionic acid.

be ascribed to agglomeration phenomena of Pt NPs when their amount exceeds a proper quantity.

3.2.2. *NOx photodegradation*

The synthesized photocatalysts were also tested for the degradation of NOx under LED irradiation.

Fig. SI.9 illustrates the results of NOx photodegradation by TiO_2, 1% Ag/TiO_2, 4%Ag/TiO_2, and 8%Ag/TiO_2. As expected, under LED, bare TiO_2 shows low efficiency towards NOx removal (30%), whereas all the three primary decorated samples (by 1%, 4%, and 8% of Ag NPs, respectively) exhibit extraordinary photoactivity [28,37]. 1%Ag/TiO_2 is able to degrade 77% of initial NOx. Increasing the Ag loading on TiO_2 to 4%, the percentage of NOx abatement reaches 81% and remains quite constant for further increase in the Ag content (8%Ag/TiO_2 removes 85% of initial NOx). LSPR absorption in Ag NPs is the main effect that makes this photocatalyst active under LED irradiation.

Concerning the doubly decorated materials (Fig. 8), an inverse trend is observed with respect to that previously observed for PA photodegradation. In fact, now the presence of Au NPs (0.1%Au @Ag/TiO_2) promotes a more significant NOx abatement, reaching >90% of NOx removal in 3 h of LED irradiation. In contrast, the secondary decoration with Pt NPs (0.1%Pt @Ag/TiO_2, 0.1% AuPt @Ag/TiO_2) partially depresses the activity of the catalyst, leading to a maximum degradation value of the 70% and 60%.for 0.1%Pt @Ag/TiO_2, 0.1%AuPt @Ag/TiO_2, respectively.

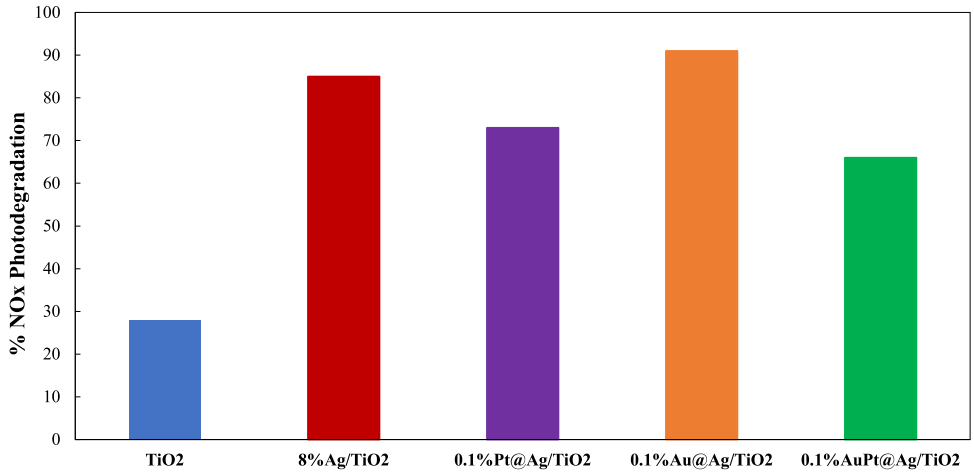

Fig. 8. Percentage of NOx photodegradation by TiO_2, 8%Ag/TiO_2, 0.1%Pt@Ag/TiO_2, 0.1%Au@Ag/TiO_2 and 0.1%AuPt @Ag/TiO_2.

The positive effect of Au NPs, towards NOx removal was already reported in some studies, demonstrating that Au NPs were beneficial for absorbing visible light. However, the present results demonstrate that diverse phenomena concur with the positive effect of Au NPs decoration. The increased activity of the gold-decorated photocatalyst might result from a high tolerance of Au NPs to HNO_3 produced on the surface of the catalyst, as recently demonstrated by Luna et al. for similar systems. [38]

4. Conclusion

In the present research, the decomposition of propionic acid, as one of the leading organic compounds in odors-polluted areas, and NOx, as model molecules for inorganic air pollutants, in the presence of both primary (Ag) and secondary (Au, Pt, and AuPt) noble metals-modified micro-sized TiO_2 under LED has been investigated. Concerning photocatalyst preparation, a sustainable approach based on the use of noble metals-enriched wastewater has been proposed.

It was demonstrated that the presence of metallic impurities (mainly Cu) in the wastewater used for the preparation of the photocatalysts has a beneficial effect on the materials' photoactivity, probably acting in the reduction of the holes-electrons recombination and, consequently, enhancing the lifetime of the photogenerated charges.

Moreover, the results demonstrated that the secondary decoration of Ag/TiO_2 with Pt NPs in small amounts causes an enhancement in the photocatalytic properties towards both PA and NOx degradation due to the localized surface plasmon resonance (LSPR) effect from Ag NPs and the "electron sink" effect from Pt. On the contrary, the effect of Au NPs is strongly related to the type of pollutant to be degraded. In fact, the presence of gold suppresses the photoactivity of the catalyst towards PA abatement because of the strong surface adsorption of PA molecules on the catalyst surface that blocks the active sites reducing their photoactivity. On the contrary, when employed in the NOx removal, 0.1%Au @Ag/TiO_2 shows the highest activity, probably for the greater chemical resistance of gold to HNO_3 produced on its surface.

Funding

This research did not receive any specific grant from funding agencies in the public, commercial, or not-for-profit sectors.

CRediT authorship contribution statement

Niloofar Haghshenas: Methodology, Formal analysis, Investigation, Data curation, Writing – original draft. **Ermelinda Falletta:** Conceptualization, Methodology, Data curation, Validation, Supervision, Writing – review & editing. **Giuseppina Cerrato:** Formal analysis, Data curation, Writing – review & editing. **Alessia Giordana:** Formal analysis, Data curation. **Claudia L. Bianchi:** Conceptualization, Data curation, Supervision, Writing – review & editing, Project administration, Funding acquisition.

Declaration of Competing Interest

The authors declare that they have no known competing financial interests or personal relationships that could have appeared to influence the work reported in this paper.

Data availability

Data will be made available on request.

Acknowledgment

The authors thank Professor Mariangela Longhi, Dr. Mirko Magni and Giacomo Falcone from Università degli Studi di Milano materials characterization and experimental tests, as well as Argor-Heraeus SA from Mendrisio (CH) Switzerland for providing the metal-enriched solutions.

Appendix A. Supplementary data

Supplementary data to this article can be found online at https://doi.org/10.1016/j.catcom.2023.106728.

References

[1] R. Hu, G. Liu, H. Zhang, H. Xue, X. Wang, P.K.S. Lam, Odor pollution due to industrial emission of volatile organic compounds: a case study in Hefei, China, J. Clean. Prod. 246 (2020), 119075, https://doi.org/10.1016/j.jclepro.2019.119075.

[2] K. Liu, Y. Chen, N. Xiao, X. Zheng, M. Li, Effect of humic acids with different characteristics on fermentative short-chain fatty acids production from waste activated sludge, Environ. Sci. Technol. 49 (2015) 4929–4936, https://doi.org/10.1021/acs.est.5b00200.

[3] A.G. James, C.J. Austin, D.S. Cox, D. Taylor, R. Calvert, Microbiological and biochemical origins of human axillary odour, FEMS Microbiol. Ecol. 83 (2013) 527–540, https://doi.org/10.1111/1574-6941.12054.

[4] S. Daikoku, M. Mitsuda, T. Tanamura, K. Uchiyama, Measuring odor threshold using a simplified olfactory measurement method, J. Hum.-Environ. Syst. 21 (2019) 1–8, https://doi.org/10.1618/jhes.21.1.

[5] S.C. Gad, Propionic acid, in: Encycl. Toxicol, Elsevier, 2014, pp. 1105–1107, https://doi.org/10.1016/B978-0-12-386454-3.00914-3.

[6] Y. Wong, Y. Li, Z. Lin, A. Kafizas, Studying the effects of processing parameters in the aerosol-assisted chemical vapour deposition of TiO2 coatings on glass for applications in photocatalytic NOx remediation, Appl. Catal. A Gen. 648 (2022), 118924, https://doi.org/10.1016/j.apcata.2022.118924.

[7] Š. Nosek, T. Ducháček, P. Magyar, J. Procházka, The role of flow structures in the effective removal of NOx pollutants by a TiO2-based coating in a street canyon, J. Environ. Chem. Eng. 11 (2023), 109758, https://doi.org/10.1016/j.jece.2023.109758.
[8] R. Kumar, P. Raizada, T. Ahamad, S.M. Alshehri, Q. Van Le, T.S. Alomar, V.-H. Nguyen, R. Selvasembian, S. Thakur, D.C. Nguyen, P. Singh, Polypyrrole-based nanomaterials: a novel strategy for reducing toxic chemicals and others related to environmental sustainability applications, Chemosphere. 303 (2022), 134993, https://doi.org/10.1016/j.chemosphere.2022.134993.
[9] A. Sudhaik, P. Raizada, P. Shandilya, D.-Y. Jeong, J.-H. Lim, P. Singh, Review on fabrication of graphitic carbon nitride based efficient nanocomposites for photodegradation of aqueous phase organic pollutants, J. Ind. Eng. Chem. 67 (2018) 28–51, https://doi.org/10.1016/j.jiec.2018.07.007.
[10] A. Fujishima, K. Honda, Electrochemical photolysis of water at a semiconductor electrode, Nature. 238 (1972) 37–38, https://doi.org/10.1038/238037a0.
[11] L.M. Betts, F. Dappozze, C. Guillard, Understanding the photocatalytic degradation by P25 TiO 2 of acetic acid and propionic acid in the pursuit of alkane production, Appl. Catal. A Gen. 554 (2018) 35–43, https://doi.org/10.1016/j.apcata.2018.01.011.
[12] N. Rozman, P. Nadrah, R. Cornut, B. Jousselme, M. Bele, G. Dražić, M. Gaberšček, Š. Kunej, A.S. Škapin, TiO2 photocatalyst with single and dual noble metal co-catalysts for efficient water splitting and organic compound removal, Int. J. Hydrog. Energy 46 (2021) 32871–32881, https://doi.org/10.1016/j.ijhydene.2021.07.129.
[13] A. Malankowska, M.P. Kobylański, A. Mikolajczyk, O. Cavdar, G. Nowaczyk, M. Jarek, W. Lisowski, M. Michalska, E. Kowalska, B. Ohtani, A. Zaleska-Medynska, TiO2 and NaTaO3 decorated by trimetallic au/Pd/Pt core-shell nanoparticles as efficient photocatalysts: experimental and computational studies, ACS Sustain. Chem. Eng. 6 (2018) 16665–16682, https://doi.org/10.1021/acssuschemeng.8b03919.
[14] Q. Lang, Y. Chen, T. Huang, L. Yang, S. Zhong, L. Wu, J. Chen, S. Bai, Graphene "bridge" in transferring hot electrons from plasmonic ag nanocubes to TiO2 nanosheets for enhanced visible light photocatalytic hydrogen evolution, Appl. Catal. B Environ. 220 (2018) 182–190, https://doi.org/10.1016/j.apcatb.2017.08.045.
[15] X. Zou, A. Goswami, T. Asefa, Efficient noble metal-free (electro)catalysis of water and alcohol oxidations by zinc–cobalt layered double hydroxide, J. Am. Chem. Soc. 135 (2013) 17242–17245, https://doi.org/10.1021/ja407174u.
[16] C.M. Pecoraro, M. Bellardita, V. Loddo, F. Di Franco, L. Palmisano, M. Santamaria, A facile way to synthesize noble metal free TiO2 based catalysts for glycerol photoreforming, J. Ind. Eng. Chem. 118 (2023) 247–258, https://doi.org/10.1016/j.jiec.2022.11.010.
[17] P.S. Vankar, D. Shukla, Biosynthesis of silver nanoparticles using lemon leaves extract and its application for antimicrobial finish on fabric, Appl. Nanosci. 2 (2012) 163–168, https://doi.org/10.1007/s13204-011-0051-y.
[18] A. Šileikaitė, J. Puiso, I. Prosycevas, S. Tamulevičius, Investigation of silver nanoparticles formation kinetics during reduction of silver nitrate with sodium citrate, Medziagotyra. 15 (2009).
[19] K. Shameli, M. Bin Ahmad, S.D. Jazayeri, P. Shabanzadeh, P. Sangpour, H. Jahangirian, Y. Gharayebi, Investigation of antibacterial properties silver nanoparticles prepared via green method, Chem. Cent. J. 6 (2012) 73, https://doi.org/10.1186/1752-153X-6-73.
[20] L. Rodríguez-Sánchez, M.C. Blanco, M.A. López-Quintela, Electrochemical synthesis of silver nanoparticles, J. Phys. Chem. B 104 (2000) 9683–9688, https://doi.org/10.1021/jp001761r.
[21] B. Yin, H. Ma, S. Wang, S. Chen, Electrochemical synthesis of silver nanoparticles under protection of poly(N -vinylpyrrolidone), J. Phys. Chem. B 107 (2003) 8898–8904, https://doi.org/10.1021/jp0349031.
[22] M. Stucchi, D. Meroni, G. Safran, A. Villa, C.L. Bianchi, L. Prati, Noble metal promoted TiO2 from silver-waste valorisation: synergism between ag and au, Catalysts. 12 (2022) 235, https://doi.org/10.3390/catal12020235.
[23] C.L. Bianchi, S. Gatto, C. Pirola, A. Naldoni, A. Di Michele, G. Cerrato, V. Crocellà, V. Capucci, Photocatalytic degradation of acetone, acetaldehyde and toluene in gas-phase: comparison between nano and micro-sized TiO2, Appl. Catal. B Environ. 146 (2014) 123–130, https://doi.org/10.1016/j.apcatb.2013.02.047.
[24] M. Stucchi, C.L. Bianchi, C. Argirusis, V. Pifferi, B. Neppolian, G. Cerrato, D. C. Boffito, Ultrasound assisted synthesis of ag-decorated TiO2 active in visible light, Ultrason. Sonochem. 40 (2018) 282–288, https://doi.org/10.1016/j.ultsonch.2017.07.016.
[25] E. Falletta, C. Della Pina, M. Rossi, Q. He, C.J. Kiely, G.J. Hutchings, Enhanced performance of the catalytic conversion of allyl alcohol to 3-hydroxypropionic acid using bimetallic gold catalysts, Faraday Discuss. 152 (2011) 367, https://doi.org/10.1039/c1fd00063b.
[26] G. Cappelletti, S. Ardizzone, C.L. Bianchi, S. Gialanella, A. Naldoni, C. Pirola, V. Ragaini, Photodegradation of pollutants in air: enhanced properties of Nano-TiO2Prepared by ultrasound, Nanoscale Res. Lett. 4 (2009) 97, https://doi.org/10.1007/s11671-008-9208-3.
[27] R. López, R. Gómez, Bandgap energy estimation from diffuse reflectance measurements on sol–gel and commercial TiO2: a comparative study, J. Sol-Gel Sci. Technol. 61 (2012) 1–7, https://doi.org/10.1007/s10971-011-2582-9.
[28] G. Cerrato, F. Galli, D.C. Boffito, L. Operti, C.L. Bianchi, Correlation preparation parameters/activity for microTiO2 decorated with SilverNPs for NOx photodegradation under LED light, Appl. Catal. B Environ. 253 (2019) 218–225, https://doi.org/10.1016/j.apcatb.2019.04.056.
[29] C. Su, L. Liu, M. Zhang, Y. Zhang, C. Shao, Fabrication of ag/TiO2 nanoheterostructures with visible light photocatalytic function via a solvothermal approach, CrystEngComm. 14 (2012) 3989, https://doi.org/10.1039/c2ce25161b.
[30] H. Jia, S. Gao, Y. Duan, Q. Fu, X. Che, H. Xu, Z. Wang, J. Cheng, Investigation of health risk assessment and odor pollution of volatile organic compounds from industrial activities in the Yangtze River Delta region, China, Ecotoxicol. Environ. Saf. 208 (2021), 111474, https://doi.org/10.1016/j.ecoenv.2020.111474.
[31] M.V. Dozzi, A. Candeo, G. Marra, C. D'Andrea, G. Valentini, E. Selli, Effects of photodeposited gold vs platinum nanoparticles on N,F-doped TiO 2 photoactivity: a time-resolved photoluminescence investigation, J. Phys. Chem. C 122 (2018) 14326–14335, https://doi.org/10.1021/acs.jpcc.8b02997.
[32] J. Shi, J. Chen, Z. Feng, T. Chen, Y. Lian, X. Wang, C. Li, Photoluminescence characteristics of TiO 2 and their relationship to the Photoassisted reaction of water/methanol mixture, J. Phys. Chem. C 111 (2007) 693–699, https://doi.org/10.1021/jp065744z.
[33] I. Alibe, K. Matori, H. Sidek, Y. Yaakob, U. Rashid, A. Alibe, M. Mohd Zaid, M. Ahmad Khiri, Effects of calcination holding time on properties of wide band gap Willemite semiconductor nanoparticles by the polymer thermal treatment method, Molecules. 23 (2018) 873, https://doi.org/10.3390/molecules23040873.
[34] Z. Wei, M. Janczarek, M. Endo, K. Wang, A. Balčytis, A. Nitta, M.G. Méndez-Medrano, C. Colbeau-Justin, S. Juodkazis, B. Ohtani, E. Kowalska, Noble metal-modified faceted anatase titania photocatalysts: octahedron versus decahedron, Appl. Catal. B Environ. 237 (2018) 574–587, https://doi.org/10.1016/j.apcatb.2018.06.027.
[35] K. Mogyorósi, Á. Kmetykó, N. Czirbus, G. Veréb, P. Sipos, A. Dombi, Comparison of the substrate dependent performance of Pt-, au- and ag-doped TiO2 photocatalysts in H2-production and in decomposition of various organics, React. Kinet. Catal. Lett. 98 (2009) 215–225, https://doi.org/10.1007/s11144-009-0052-y.
[36] Y. Wang, Q. Lai, Y. He, M. Fan, Selective photocatalytic carbon dioxide conversion with Pt@ag-TiO2 nanoparticles, Catal. Commun. 108 (2018) 98–102, https://doi.org/10.1016/j.catcom.2018.02.004.
[37] C.L. Bianchi, G. Cerrato, C. Pirola, F. Galli, V. Capucci, Photocatalytic porcelain grés large slabs digitally coated with AgNPs-TiO2, Environ. Sci. Pollut. Res. 26 (2019) 36117–36123, https://doi.org/10.1007/s11356-019-05218-7.
[38] M. Luna, J.M. Gatica, H. Vidal, M.J. Mosquera, One-pot synthesis of au/N-TiO2 photocatalysts for environmental applications: enhancement of dyes and NOx photodegradation, Powder Technol. 355 (2019) 793–807, https://doi.org/10.1016/j.powtec.2019.07.102.